Bulletin of the Seismological Society of America, Vol. 99, No. 2B, pp. 1199–1206, May 2009, doi: 10.1785/0120080267

Perspectives for Ring Laser Gyroscopes in Low-Frequency Seismology

by R. Widmer-Schnidrig and W. Zürn

Abstract Variations in the ring laser signal of the rotating Earth are caused by local rotations and by north–south tilts. Analytic expressions for the computation of synthetic seismograms for ring lasers based on normal mode summation are derived. We find that horizontal ring lasers are predominantly sensitive to torsional motion. Synthetic Sagnac signals are computed for recent earthquakes and for spherical Earth models in order to establish the general characteristics and amplitude of the expected ring laser signals. In the normal mode band north–south tilts typically amount to less than 10% of the total signal for a horizontal ring laser. The fact that no free oscillation spectra have so far been reported from ring lasers is consistent with amplitudes of our synthetic Sagnac signals and current noise levels of these sensors.

Introduction

Ring laser gyroscopes are a tool to sense local rotations with respect to an inertial reference frame having local, regional, or global origin. Successful applications include navigation of airplanes. Techniques to sense the rotations of the Earth with respect to inertial reference frames include very long baseline interferometry (VLBI), satellite and lunar laser ranging, and Global Positioning Systems for global variations of the angular velocity at daily and longer periods. At shorter periods seismic rotations have been directly observed with rotation seismometers (e.g., Teisseyre *et al.*, 2003) or indirectly inferred from dense arrays of seismometers (e.g., Igel *et al.*, 2007). Ring lasers present an alternative technique to detect local rotations over the entire seismic frequency band from 10^{-3} to 10 Hz and can be used to complement VLBI and detect fluctuations in the Earth's rotation rate at subdaily periods (e.g., Schreiber *et al.*, 2003, 2004).

Recent efforts to build ring lasers with increased sensitivity have been successful to the point that these instruments can now be used in geophysical applications. We mention three of these instruments here: the C-II (e.g., Stedman, 1997) and G0 (Rowe *et al.*, 1999) ring lasers in Christchurch, New Zealand, and the G-ring laser in Wettzell, Germany (e.g., Klügel *et al.*, 2005). Two of these instruments (C-II and G) were specifically built for Earth rotation monitoring. The C-II and G-ring lasers are horizontally installed while the G0-ring laser has a vertical sensor plane. The G-ring laser is at this time the one with the best signal-to-noise performance.

Here we concentrate on the frequency band occupied by the Earth's elastogravitational free oscillations (0.3–10 mHz) that can be routinely observed with seismometers, gravimeters, and strainmeters after earthquakes with magnitudes larger than 6.5. In this band the Earth's elastic response to earthquake sources can be very well described with synthetic seismograms computed for spherically symmetric, nonrotating, elastic and isotropic (SNREI) Earth models. The generally excellent match in amplitude and phase between observed and computed linear accelerations for $f < 6$ mHz give us the confidence that normal mode summation is also a sound basis for predicting rotations in this frequency band.

Basic Principles

In a ring laser, mirrors are used to guide light around the perimeter of a plane area. A reference to inertial space is realized by letting two beams interfere that propagate in opposite sense around the perimeter. If the ring laser were not rotating in inertial space, the interference pattern would not move past the mirrors. In an Earth bound sensor, however, the interference pattern moves past the mirrors. This is the Sagnac effect (Sagnac, 1913). The observed interference frequency is given by the Sagnac equation for active ring lasers (Aronowitz, 1971):

$$f_s = \frac{4A}{\lambda P}(\hat{n} \cdot \vec{\Omega}), \tag{1}$$

where A is the enclosed area, P the length of the perimeter, and $\vec{\Omega}$ the rotation vector. The wavelength of the laser is λ and $\hat{n}$ is a unit vector perpendicular to the plane of the ring laser, A.

The ring laser is constructed such that variations in A, P, and λ are minimized. Under these premises the variations in the Sagnac frequency, f_s, are only due to either variations in the angular velocity Ω or the angle between the vectors $\hat{n}$ and $\vec{\Omega}$ (i.e., local north–south tilts or tilts of the Earth's axis of rotation with respect to the figure axis). Both $|\vec{\Omega}|$ and the angle θ between $\hat{n}$ and $\vec{\Omega}$ can be decomposed into a large constant term and a small time variable term:

$$\Omega = \Omega_o + \delta\Omega(t), \qquad \theta = \theta_o + \delta\theta(t),$$

with θ_o the geographic colatitude of the station plus the north–south component of the tilt of the ring laser normal $\hat{n}$ against local vertical. With this decomposition of Ω and θ, we obtain

$$(\hat{n} \cdot \vec{\Omega}) = (\Omega_o + \delta\Omega)\cos(\theta_o + \delta\theta). \tag{2}$$

Assuming $\delta\Omega \ll \Omega_o$ and $\delta\theta \ll 1$ and neglecting terms of second order, we get

$$f_s(t) = \frac{4A}{\lambda P}\Omega_o\left(\cos\theta_o - \sin\theta_o\delta\theta(t) + \cos\theta_o\frac{\delta\Omega(t)}{\Omega_o}\right). \tag{3}$$

The leading term is the Sagnac frequency observed for a stable Earth rotation. The second and third terms describe variations in the Sagnac frequency due to variations in local north–south tilt and local rotations. For the *G* ring in Wettzell, the leading factor $4A/\lambda P$ is 6.3×10^6, the colatitude θ_o is 40.85°, and the constant term of f_s is 348.6 Hz.

Normal Mode Decomposition of a Seismic-Wave Field

On an SNREI Earth the seismic-wave field **u** excited by a point source at $\mathbf{r}_o$ and observed by a receiver located at **r** can be represented as a superposition of eigenmodes:

$$\mathbf{u}(\mathbf{r}_o, \mathbf{r}, t) = \sum_k \mathrm{Re}[\sigma_k^T(\mathbf{r})a_k(\mathbf{r}_o)e^{i\omega_k t}], \tag{4}$$

where k is the multiplet index denoting a multiplet of spheroidal or toroidal type of harmonic degree ℓ and overtone number n. ω_k is the degenerate eigenfrequency shared by the $2\ell + 1$ singlets, which constitute the kth multiplet. $a_k(\mathbf{r}_o)$ is the source vector made up of the $2\ell + 1$ complex singlet excitations (Dahlen and Tromp, 1998, equation 13.189) while $\sigma_k^T(\mathbf{r})$ is the transposed receiver vector made up of the $2\ell + 1$ complex singlet amplitudes evaluated at the receiver location. More specifically, if we want to compute synthetic seismograms to match the output of an accelerometer, the receiver vector contains the singlet accelerations plus small terms due to changes in gravity caused by the vertical movement of the accelerometer in the gravity field and the change in local gravity due to mass displacements (Dahlen and Tromp, 1998, equation 10.72). Likewise if we want to compute synthetic seismograms to match the Sagnac signal of a ring laser, it follows from (3) that the receiver vector contains the rotation rates and north–south tilts.

The elements of the receiver vector for a ring laser are the focus of the next section.

Elements of Receiver Vector

The Rotation Tensor. For infinitesimal deformation, the elements of the antisymmetric rotation tensor are defined as

$$\xi_{ij} = \frac{1}{2}(u_{i,j} - u_{j,i}). \tag{5}$$

If we follow the usual notation and adopt a spherical coordinate system with axes in the $\hat{r}$, $\hat{\theta}$, and $\hat{\phi}$ directions, the displacement field of an individual spheroidal singlet can be written

$$\vec{u}^S(r,\theta,\phi) = \hat{r}UY_\ell^m + \hat{\theta}V\frac{\partial Y_\ell^m}{\partial\theta} + \hat{\phi}\frac{im}{\sin(\theta)}VY_\ell^m, \tag{6}$$

where the subscripts n and ℓ identifying the multiplet are implied for the radial eigenfunctions $nU_\ell(r)$, $nV_\ell(r)$, and $nW_\ell(r)$. The Y_ℓ^ms are fully normalized spherical harmonics.

Inserting (6) into (5) we find the rotations around a vertical $\hat{r}$ axis for spheroidal singlets (see also Dahlen and Tromp, 1998, equation A.138):

$$\xi_{\theta\varphi} = 0, \tag{7}$$

for rotations around the $\hat{\theta}$ axis:

$$2\xi_{r\varphi} = -i\left(V' + \frac{V-U}{r}\right)\frac{m}{\sin(\theta)}Y_\ell^m, \tag{8}$$

and for rotations around the $\hat{\varphi}$ axis:

$$2\xi_{r\theta} = -\left(V' + \frac{V-U}{r}\right)\frac{\partial Y_\ell^m}{\partial\theta}. \tag{9}$$

Primed quantities indicate derivatives with respect to the radius r. For a toroidal singlet the displacement field is

$$\vec{u}^T(r,\theta,\phi) = \hat{\theta}\frac{im}{\sin(\theta)}WY_\ell^m - \hat{\phi}W\frac{\partial Y_\ell^m}{\partial\theta}, \tag{10}$$

and we find

$$2\xi_{\theta\varphi} = -\ell(\ell+1)\frac{W}{r}Y_\ell^m, \tag{11}$$

$$2\xi_{r\varphi} = \left(W' + \frac{W}{r}\right)\frac{\partial Y_\ell^m}{\partial\theta}, \tag{12}$$

$$2\xi_{r\theta} = -i\left(W' + \frac{W}{r}\right)\frac{m}{\sin(\theta)}Y_\ell^m. \tag{13}$$

Equations (7) and (11) imply that horizontal ring lasers, such as the G ring in Wettzell, sense only rotations induced by torsional motion such as horizontally polarized shear waves and Love waves.

North–South Tilts. Tilting of the ring laser also leads to a first order perturbation of the Sagnac frequency. So far ring lasers have been either installed on horizontal floors (e.g.,

the G ring, Wettzell, Germany, see Klügel *et al.*, 2005) or mounted against vertical walls (the G0 ring in Christchurch, New Zealand, see, e.g., Stedman, 1997). For horizontally mounted sensors the relevant spatial derivatives for north–south tilt are

$$\frac{\partial u_r}{\partial \theta} = U \frac{\partial Y_\ell^m}{\partial \theta}. \tag{14}$$

Thus horizontal ring lasers are only tilted by spheroidal modes. For the tilting of a southward facing, vertical wall we get

$$\frac{\partial u_\theta}{\partial r} = V' \frac{\partial Y_\ell^m}{\partial \theta} + \frac{im}{\sin(\theta)} W' Y_\ell^m, \tag{15}$$

implying that both spheroidal and toroidal modes contribute to the tilting of such a wall-mounted sensor.

In Figures 1 and 2 the contribution of north–south tilts and rotations to the observed perturbation of the Sagnac frequency are compared for one particular event/station pair: the 2002 M_w 7.9 Denali event recorded in Wettzell. In this case the root mean square (rms) amplitude of the tilt amounts to 2.5% of the rotation signal. Note that this number strongly depends on the source mechanism and the location of the receiver with respect to the radiation pattern of the source. For a double-couple source the nodal planes for the Rayleigh- and Love-wave radiation patterns are offset by 45°; thus a horizontal ring laser situated on the nodal plane

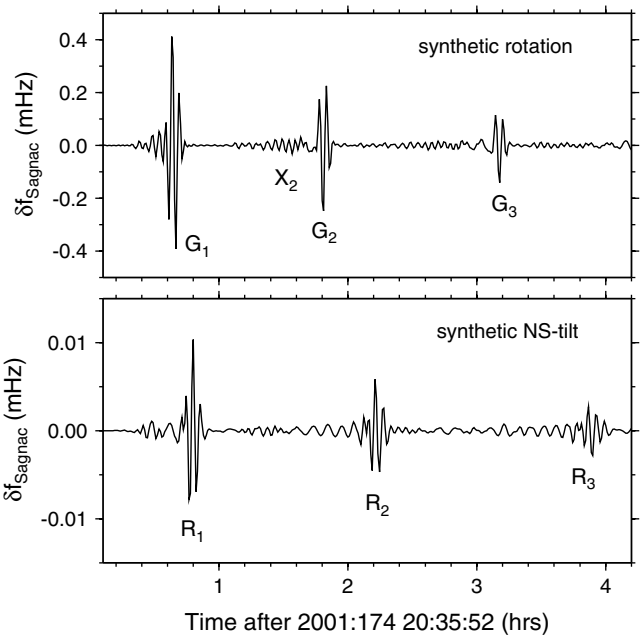

Figure 1. Time-domain comparison of synthetic seismograms simulating the M_w 7.9 Denali event (3 November 2002) and illustrating the relative contribution of rotation rate (upper panel) and tilt (lower panel) to the Sagnac signal at Wettzell. Note the different scales on the axes. For the signals shown the rms amplitude of the tilt amounts to 2.5% of the rotation signal. While the rotation signal is dominated by the fast and compact Love-wave packets the tilt signal is dominated by the slower and more strongly dispersed Rayleigh waves.

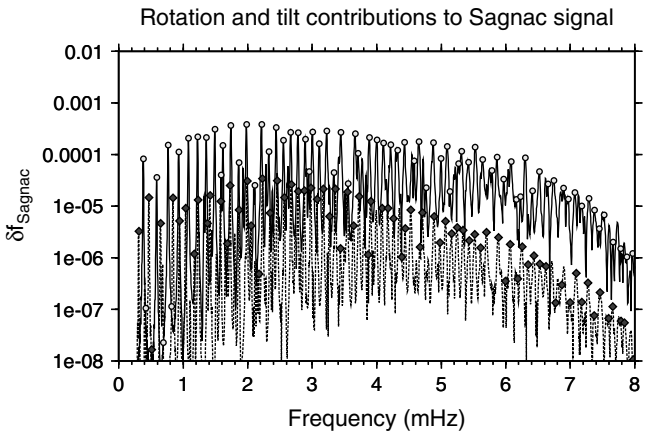

Figure 2. Frequency-domain comparison of the signals from Figure 1. The spectrum of rotation consists of toroidal modes only (open circles) while the spectrum of north–south tilt is solely made up of spheroidal modes (black diamonds). When averaged over 0.5 mHz wide frequency bands, the contribution of the tilt decreases from 10% at 1 mHz to 2.5% at 6 mHz.

of the Love-wave radiation pattern would only see tilt, while a ring laser situated on a Rayleigh-wave nodal plane would sense only rotation.

More generally one can compare the receiver vector elements for rotation (equation 11) and tilt (equation 14) in the asymptotic limit for large ℓ or equivalently for short wave lengths. While the receiver vector elements are rapidly oscillating functions of the colatitude θ one can still compare their average power. We find that the ratio of rotation over tilt is proportional to ℓ so that overall the tilt contribution to seismically induced Sagnac frequency variations decreases with frequency. This behavior can also be seen in Figure 2.

Local Cartesian Approximation

If we use a Cartesian coordinate system to describe wave propagation in a locally flat medium the particle displacement of a transversely polarized plane shear wave of *SH* type propagating in the x direction is given by

$$\vec{u} = \begin{pmatrix} 0 \\ u_y \\ 0 \end{pmatrix} W(z) e^{i(\omega t - k_x x)}. \tag{16}$$

The particle accelerations associated with this wave are

$$\ddot{u}_y = -\omega^2 u_y W(z) e^{i(\omega t - k_x t)}, \tag{17}$$

while the angles of the associated infinitesimal rigid rotations are

$$\vec{\xi} = \begin{pmatrix} \xi_x \\ \xi_y \\ \xi_z \end{pmatrix} = \frac{1}{2} \begin{pmatrix} \frac{\partial u_y}{\partial z} - \frac{\partial u_z}{\partial y} \\ \frac{\partial u_z}{\partial x} - \frac{\partial u_x}{\partial z} \\ \frac{\partial u_x}{\partial y} - \frac{\partial u_y}{\partial x} \end{pmatrix} = \frac{1}{2} \begin{pmatrix} \frac{\partial u_y}{\partial z} \\ 0 \\ -\frac{\partial u_y}{\partial x} \end{pmatrix}.$$

For the quantity sensed by a horizontal ring laser, namely the angular velocity around the vertical axis, we get

$$\dot{\xi}_z = \Omega_z = -\frac{1}{2}\omega k_x u_y W(z) e^{i(\omega t - k_x x)}, \tag{18}$$

so that

$$\frac{\ddot{u}_y}{\Omega_z} = 2\frac{\omega}{k_x} = 2c(\omega). \tag{19}$$

Thus for plane *SH* waves the transversal acceleration and the rotation around a vertical axis are simply connected by the (frequency dependent) local phase velocity $c = \omega/k_x$.

A similar equation was already derived for strains and accelerations by Mikumo and Aki (1979). These authors suggested to measure local phase velocities by installing horizontal strain meters and vertical inertial seismometers at the same location. This technique strongly relies on the assumption of plane waves (see Wielandt [1993] for effects of nonplanarity).

The relation (19) also holds approximately on a spherical Earth. This is demonstrated in Figure 3 where full mode synthetics for the transversal acceleration and angular velocity are compared. Equation (19) has also been verified for earthquake data by Igel *et al.* (2007).

Data

Earthquake Signals

Recordings of the M_w 8.1 2007 Kuriles event (epicentral distance, Δ, equals 80°, back azimuth equals 25°) from the G ring and the STS-2 seismometer at Wettzell are compared in Figures 4 and 5. From the different data acquisition systems connected to the G ring we have found that the frequency counter (SR1E data stream) sampled at 5 Hz is best suited for studies in the normal mode band. From the STS-2 seismometer we use the long-period output (LH streams) sampled at 1 Hz.

To compare the signal content of the recordings in the time domain, we first convert the seismometer output to ground acceleration and then low-pass filter the two datasets with zero-phase filters. We also calculate the transversal component from the north–south and east–west seismometer outputs as this component should most closely match the ring laser output (equation 19).

By successively lowering the corner frequency from 400 to 40, 10, and 5 mHz, we get the four traces in Figures 4 and 5. The gain has been increased from top to bottom by the same factors in the two figures to allow for a fair comparison.

While the top two traces are very similar for both sensors, a first difference is noticeable in the case with a 10 mHz corner frequency (third trace): the noise level before the event and after the first Love wave (G_1) are hardly different for the ring laser (Fig. 4). In the bottom trace, which only contains signal below 5 mHz, no Love waves can be reliably detected. In contrast, the third trace of Figure 5 shows a very clear signal onset. In the bottom trace, the tilt noise prior to the event can be seen, but still the Love waves G_1 and G_2, as well as the overtone phase X_2, are present with good signal-to-noise ratio.

Igel *et al.* (2005) compared rotations observed with the G-ring laser to accelerations observed with collocated STS-2 seismometer from the M_w 8.1 Tokachi-oki (23 September

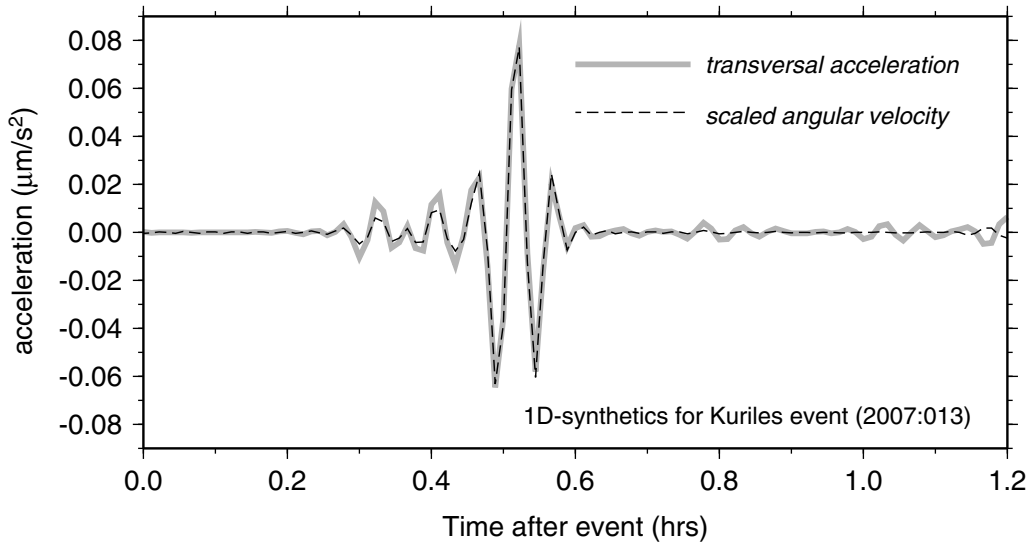

Figure 3. Comparison of synthetic seismograms for the large (M_w 8.1) Kuriles event of 13 January 2007. The synthetics were computed using the mode summation method and the Preliminary Reference Earth Model (Dziewonski and Anderson, 1981). Shown are the scaled local rotation rate around a vertical axis and the horizontal acceleration perpendicular to the direction of propagation. The scale factor is $2c$ with $c = 4.8$ km/sec, the phase velocity for Love waves in the Preliminary Reference Earth Model. Note how for the earlier arriving overtones (0.25–0.45 hr after the event) a higher value for the phase velocity is needed to make the two synthetics match.

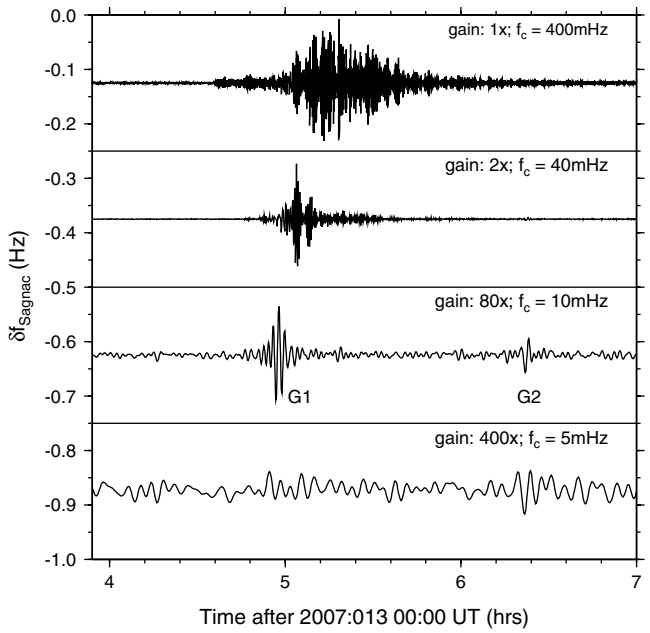

Figure 4. Time-domain analysis of the 2007 Kuriles event recorded by the G ring at Wettzell. The variation of the Sagnac frequency is low-pass filtered with successively lower corner frequency f_c. For clarity the traces are offset and the gains individually adjusted.

2003) earthquake. They determined the phase velocities of shear waves and Love waves as a function of arrival time and obtained nice results in agreement with equation (19).

Noise Spectra

Because ring lasers and horizontal seismometers measure intrinsically different quantities, a meaningful comparison can only be made in the context of a particular task. Restricting ourselves to the most common case of horizontally installed ring lasers, we ask which sensor is the better detector for horizontally polarized shear waves. For this type of waves, equation (19) can be used to convert angular velocities sensed by a ring laser into equivalent horizontal accelerations.

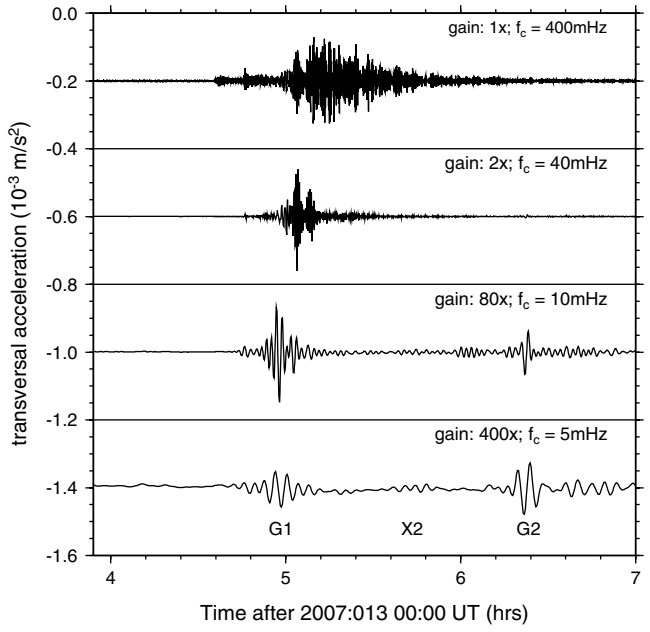

Figure 5. Same as Figure 4 but for the transversal acceleration as recorded by the STS-2 seismometer at Wettzell.

In Figure 6, power spectral densities (psds) of simultaneous datasets free of large earthquakes from the G ring and the three components of the STS-2 seismometer at Wettzell are compared. The STS-2 seismometer at Wettzell is installed less than 260 m away from the G ring and should sense the same wave field given the frequency band considered here.

The psd of the G ring is flat and shows none of the geophysical signals permanently present in this frequency band: $1/f$-type tilting due to atmospheric loading such as seen on horizontal inertial sensors (seismometers and tiltmeters) or the rotational component of Love waves, which have been shown to be a constituent of the marine microseisms at the nearby (135 km) Gräfenberg seismic array (Friedrich *et al.*, 1998). This signal should peak near 150 mHz.

Based on data from 2006/2007 we find that in the normal mode band (1–10 mHz) the STS-2 inertial seismometer at Wettzell is an *SH*-wave detector that is between 20 and 50 dB more sensitive than the collocated G-ring laser. This large span is primarily due to the fact that the noise level on horizontal component seismometers depends on local weather conditions and is therefore highly variable. This variability can also be seen in the two Figures 6 and 7.

While seismometers installed in mine observatories may exhibit lower horizontal noise levels than at Wettzell, we interpret the flat noise level for the G ring in Figure 6 as a clear sign that the sensitivity of the G ring is not limited by tilt noise in the millihertz band.

Marine Microseisms

Noting that the secondary microseism peak in Figure 6 as observed with the seismometer reaches the noise level of the G ring of −120 dB, we carried out a search for the largest microseism storm in the winter of 2006/2007. The result for a North Atlantic storm on 22 February 2007 is summarized in Figure 7 and demonstrates that the G ring is indeed capable of detecting at least the largest microseism signals. The secondary microseism peak at 0.125 Hz (8 sec period) observed with the G ring is smaller by 12 dB (a factor of 4 in amplitude) relative to the vertical acceleration as seen by the STS-2. This is in rough agreement with the findings of Friedrich *et al.* (1998) who used three component broadband data from two nearby seismic arrays to separate marine microseisms into coherent Rayleigh and Love waves. For other large microseism storms they found an amplitude ratio of 4 : 1 for coherent Rayleigh to Love energy (6 dB). Note that the time window used for Figure 6 contains microseisms from multiple storms in the North Atlantic. This explains

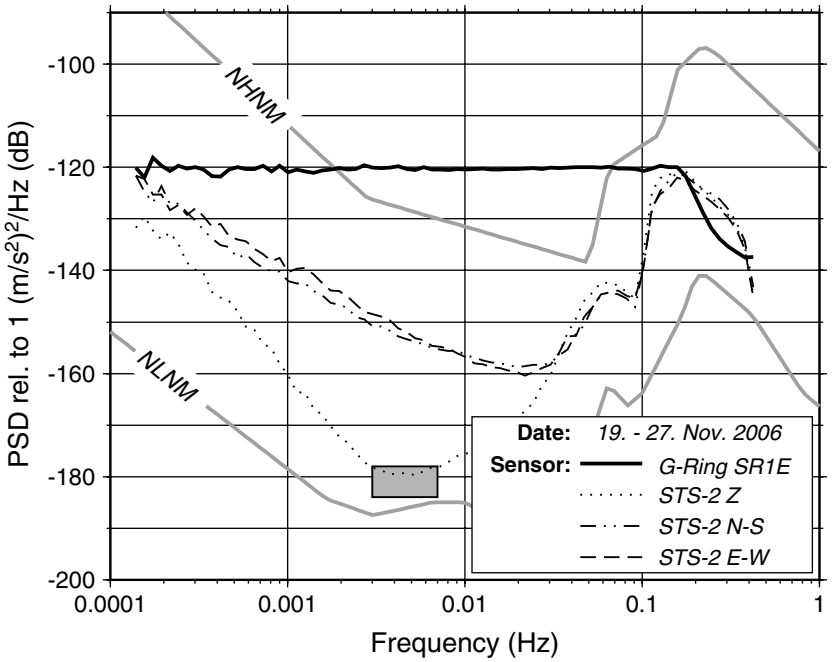

Figure 6. Comparison of acceleration psds for different sensors at Wettzell. Data are from the G ring and the STS-2 seismometer. For reference the new low- and high-noise model of Peterson (1993) for vertical component seismic noise is also shown. The gray rectangle indicates the frequency band and signal power of the horizontal hum, which can, at least in principle, also be detected with a ring laser. The phase velocity used to convert the Sagnac signal into accelerations (equation 19) is $c = 5$ km/sec

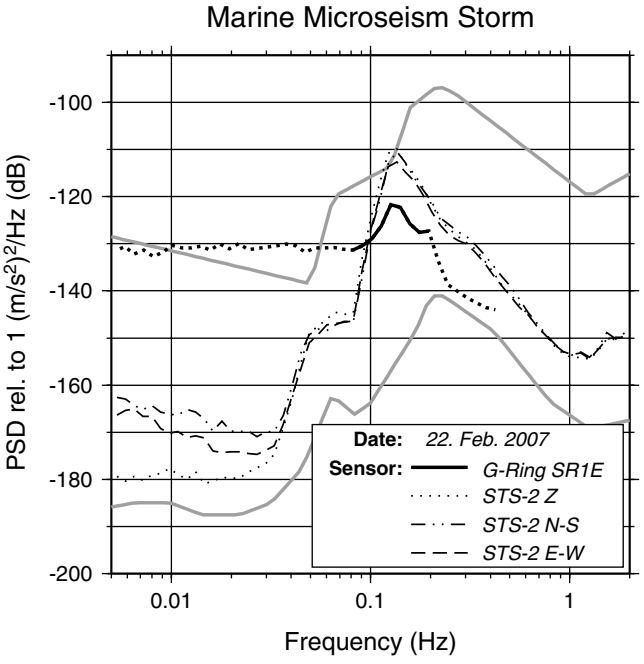

Figure 7. Figure similar to Figure 6 but based on a 24 hr long time window containing a large marine microseismic storm. The phase velocity used to convert the Sagnac signal into accelerations (equation 19) is $c = 3.7$ km/sec. This velocity is only valid in the band of the secondary microseism peak indicated by the solid line (0.08–0.2 Hz).

why the secondary microseism peak in Figure 7 is only 10 dB higher than in Figure 6.

Permanent Background Free Oscillations: the Hum

While horizontal seismometers are known for their notoriously high-noise level—presumably due to tilts from atmospheric loading—Kurrle and Widmer-Schnidrig (2008) still managed to detect the permanently excited background free oscillations (also known as the hum of the Earth) in a 10 yr long dataset of horizontal component seismic data in the band 3–7 mHz. They found that these oscillations do not only consist of fundamental spheroidal modes like the vertical component hum but also contain the fundamental toroidal modes. A surprise in this study was that the horizontal amplitudes of both spheroidal and toroidal modes were equally large with an estimated rms amplitude of 3 pm/sec^2 of the individual multiplets. The equivalent psd of this signal corresponds to −190 dB in Figure 6. In the presence of noise this signal gets nonlinearly amplified so that it can be detected up to approximately −180 dB before it completely drowns in the noise. Converted into rotations using equation (19), we find a value of $4 \times 10^{-12}\ \Omega_o$ for the rotational noise floor in the 3–7 mHz band provided by the toroidal hum.

Limitation of Ring Lasers by Tilt Noise

At periods longer than 100 sec, acceleration noise on horizontal component seismometers is dominated by tilt (Pe-

terson, 1993; Zürn *et al.*, 2007) while at shorter periods inertial accelerations constitute the dominant effect. Tilt, α, is related to apparent horizontal accelerations, $\ddot{u}_x$, by

$$\alpha = \frac{\ddot{u}_x}{g}, \tag{20}$$

where g is local gravity ($g \simeq 9.8$ m/sec^2) and the small tilt, α, is the angle between the direction of local gravity and the normal of the sensor plane. Thus, before a Love wave can be detected with a horizontal seismometer, the inertial acceleration due to the Love wave must exceed $\ddot{u}_x^{\text{Love}} > g\alpha$, where α is the tilt noise.

Let us now ask how the same tilt noise competes with rotations from Love waves in the case of a horizontal ring laser. Tilt noise estimated from the north–south component of the STS-2 seismometer at Wettzell can then be translated into an equivalent perturbation of the Sagnac frequency based on equation (3). Note that at quiet stations this tilt is mostly caused by spheroidal oscillations or atmospheric loading (e.g., Zürn *et al.*, 2007).

The Sagnac perturbation due to rotations from a passing Love wave can be computed based on equations (3) and (19):

$$\delta f_s^{\text{rotation}} = \frac{4A}{\lambda P} \cdot \Omega_o \cdot \frac{\ddot{u}_x}{2c} \cos\theta_o, \tag{21}$$

while the Sagnac perturbation due to tilt noise α is

$$\delta f_s^{\text{tilt}} = \frac{4A}{\lambda P} \cdot \Omega_o \cdot \alpha \cdot \sin\theta_o. \tag{22}$$

The signal-to-noise ratio p^{RL} with which the Love wave is seen by the ring laser then becomes

$$p^{RL} = \frac{\delta f_s^{\text{rotation}}}{\delta f_s^{\text{tilt}}} = \frac{\ddot{u}_x}{2c} \cdot \cot\theta_o \cdot \frac{1}{\Omega_o} \cdot \frac{1}{\alpha}. \tag{23}$$

For a collocated horizontal seismometer the inertial acceleration due to the Love waves is $\ddot{u}_x$ while the tilt noise is αg so that the signal-to-noise ratio for this type of instrument becomes

$$p^{BB} = \frac{\ddot{u}_x}{\alpha g}. \tag{24}$$

Comparing now the signal-to-noise ratio with which the Love wave is seen by the two types of sensors, we get

$$\frac{p^{RL}}{p^{BB}} = \frac{g\cot\theta_o}{2c\Omega_o}. \tag{25}$$

Assuming an average phase velocity $c \simeq 5$ km/sec and a sensor installed at midlatitudes for which $|\cot\theta_o| \simeq 1$ we find that $p^{RL}/p^{BB} \simeq 10$. Thus, the smallest Love wave that can in principle be detected with a horizontal ring laser is a factor of 10 (20 dB) smaller in amplitude than the smallest Love wave detectable with a horizontal component seismometer. Love waves with smaller amplitudes cannot be detected with a ring laser as they would drown in the tilt noise. This discussion assumes an idealized ring laser for which tilt noise is the dominant noise source and sensor self noise is negligible.

To address the tilt sensitivity of the G ring the tilt of its pier is measured with Lippmann tiltmeters so that the Sagnac signal can in principle be corrected for tilt. The crucial question then concerns the self noise of the Lippmann tiltmeters. This can be estimated by inspecting the coherence of the six tiltmeters installed on the G-ring pier. If tilt were measured with STS-2 seismometers on the G-ring pier, one could use the STS-2 self noise estimated in Wielandt and Widmer-Schnidrig (2002) and work from there.

Let us now extend this line of arguments to wall-mounted ring lasers, which sense rotations due to both spheroidal and toroidal modes. As a lower bound on the tilt induced Sagnac signal, one can use the same tilts measured with horizontal component seismometers. But the smallest spheroidal modes detectable with a seismometer must only exceed the comparably much lower noise level of vertical component seismometers (see Fig. 6). In fact the separation between the noise levels on horizontal and vertical component seismometers is typically 20 dB at periods longer than 100 sec. In spite of the lack of a comparably simple expression analogous to equation (3) the aforementioned lower noise level on vertical component accelerometers leads us to speculate that it is very unlikely that vertical ring lasers can be made into more sensitive spheroidal mode detectors than vertical component seismometers or gravimeters.

Tilt noise in the aftermath of earthquakes has two sources: (1) tilts from the spheroidal modes that lead to a deformation of the Earth's surface and (2) other sources such as atmospheric phenomena. These latter sources are highly variable. For any ring laser, the relative size of the tilt and rotation signals from an earthquake depends on the source mechanism. Furthermore, because on average the quality factor of spheroidal modes is higher than for toroidal modes, the tilt contribution in the Sagnac signal of a horizontally installed ring laser will increase with increasing time after the event. In other words we expect signal generated tilt noise to increase with time after an earthquake.

According to Zürn *et al.* (2007) typical amplitudes of atmospherically caused tilts as observed at quiet underground stations are 5×10^{-8} msec^{-2}/hPa. Thus, ring laser tilt noise, α, due to atmospheric pressure fluctuations, p, can be $g\alpha/p = 5 \times 10^{-8}$ msec^{-2}/hPa. Depending on the atmospheric phenomenon causing tilt noise, the associated Newtonian attraction and inertial effects limit the possibilities to correct this noise using tiltmeters such as installed on the G ring in Wettzell.

Conclusions

Clearly, ring laser gyroscopes can measure a variety of very interesting geophysical signals of local, regional, and

global origin. Here, we have inspected signals from large teleseisms and large marine microseism storms. Considering the normal mode or surface-wave perspective only and assuming plane wavefronts, ring laser gyroscopes do not observe fundamentally new observables because the ring laser signal can be computed from the signals of collocated broadband seismometers if the local phase velocities of the waves are known. However, if these two conditions are not met (planarity of wavefront, knowledge of phase velocity) then information may be gleaned (albeit with difficulty) from the comparison of collocated ring laser and seismometer records.

Because at low frequencies ($f < 5$ mHz) horizontal seismometers are limited by tilt noise, there exists the possibility for obtaining superior torsional mode spectra with ring lasers provided that their self noise is further reduced.

While the comparison of seismometers and ring lasers in Figures 4, 5, and 6 is highly unfavorable for the ring laser, recent improvements in the processing of the Sagnac signal based on a different demodulation technique have dramatically lowered the self noise of the G ring in the frequency band relevant for local earthquake signals (0.1–10 Hz) (Flaws, 2003; Flaws *et al.*, 2003). Thus, it seems quite likely that further improvements are also possible in the frequency band relevant for the study of normal modes.

Data and Resources

Data from the ring laser gyroscope at Wettzell (G ring) were provided by Th. Klügel (BKG, Wettzell), available at http://www.fs.wettzell.de (last accessed November 2008). Data from the broadband STS-2 seismometer at Wettzell were obtained from the Seismologisches Zentralobservatorium Gräfenberg (SZGRF) at www.szgrf.bgr.de (last accessed November 2008).

All plots were made using the Generic Mapping Tools version 4.3.1 (www.soest.hawaii.edu/gmt; Wessel and Smith, 1991).

Acknowledgments

We thank Th. Klügel (BKG, Wettzell) and U. Schreiber (TUM, Wettzell) for making the data from the G ring laser available and the network center SZGRF of the German Regional Seismic Network (GRSN) for the seismic data from Wettzell. The constructive comments of two anonymous reviewers helped to improve the manuscript and are gratefully acknowledged.

References

Aronowitz, A. (1971). The laser gyro, in *Laser Applications*, Academic Press, New York, 133–200.

Dahlen, F., and J. Tromp (1998). *Theoretical Global Seismology*, Princeton University Press, Princeton, New Jersey.

Dziewonski, A., and D. Anderson (1981). Preliminary reference Earth model, *Phys. Earth Planet. Interiors* **25,** 297–356.

Flaws, A. (2003). *Ring laser technology for seismic applications*, *Master's Thesis*, University of Canterbury, New Zealand.

Flaws, A., A. Cochard, U. Schreiber, A. Velikoseltsev, and H. Igel (2003). Reaching seismic frequency requirements with a ring laser gyroscope, Poster presented at the *29th Arbeitsgruppe Seismologie*, Fürstenfeldbruck, 17–19 September 2003.

Friedrich, A., F. Krüger, and K. Klinge (1998). Ocean generated microseismic noise located with the Gräfenberg array, *J. Seism.* **2,** 47–64.

Igel, H., A. Cochard, J. Wassermann, A. Flaws, U. Schreiber, A. Velikoseltsev, and N. Pham Dinh (2007). Broad-band observations of earthquake-induced rotational ground motions, *Geophys. J. Int.* **168,** 182–197.

Igel, H., U. Schreiber, A. Flaws, B. Schuberth, A. Velikoseltsev, and A. Cochard (2005). Rotational motions induced by the *M* 8.1 Tokachi-Oki earthquake, September 25, 2003, *Geophys. Res. Lett.* **32,** L08309, doi 10.1029/2004GL022336.

Klügel, T., W. Schlüter, U. Schreiber, and M. Schneider (2005). Großringlaser zur kontinuierlichen Beobachtung der Erdrotation, *Z. Vermess.* **130,** no. 2, 99–108.

Kurrle, D., and R. Widmer-Schnidrig (2008). The horizontal hum of the earth: a global background of spheroidal and toroidal modes, *Geophys. Res. Lett.* **35,** L06304, doi 10.1029/2007GL033125.

Mikumo, T., and K. Aki (1979). Determination of local phase velocity by intercomparison of seismograms from strain and pendulum instruments, *J. Geophys. Res.* **69,** 721–731.

Peterson, J. (1993). Observations and modeling of seismic background noise, *U.S. Geol. Surv., Open-File Rept. 93-322*, 1–45.

Rowe, C. H., U. K. Schreiber, S. J. Cooper, B. T. King, M. Poulten, and G. E. Stedman (1999). Design and operation of a very large ring laser gyroscope, *Appl. Opt.* **38,** 2516–2523.

Sagnac, M. G. (1913). La démonstration de l'existence de l'éther lumineux a travers les mesures d'un intérferomètre en rotation, *C. R. l'Acad. Sci.* **157,** 708–718.

Schreiber, U., T. Klügel, and G. E. Stedman (2003). Earth tide and tilt detection by a ring laser gyroscope, *J. Geophys. Res.* **108,** no. B2, 2132, doi 10.1029/2001JB000569.

Schreiber, U., A. Velikoseltsev, M. Rothacher, T. Klügel, G. E. Stedman, and D. L. Wiltshire (2004). Direct measurement of diurnal polar motion by ring laser gyroscopes, *J. Geophys. Res.* **109,** no. B6, B06405, doi 10.1029/2003JB002803.

Stedman, G. E. (1997). Ring laser tests of fundamental physics and geophysics, *Rep. Progr. Phys.* **60,** no. 6, 615–688.

Teisseyre, R., J. Suchcicki, K. Teisseyre, J. Wiszniowski, and P. Palangio (2003). Seismic rotation waves: basic elements of theory and recording, *Ann. Geophys.* **46,** 671–685.

Wessel, P., and H. F. Smith (1991). Free software helps map and display data, *EOS Trans. AGU* **72,** 441.

Wielandt, E. (1993). Propagation and interpretation of non-plane waves, *Geophys. J. Int.* **113,** 45–53.

Wielandt, E., and R. Widmer-Schnidrig (2002). Seismic sensing and data acquisition in the GRSN, in *Ten Years of the German Regional Seismic Network (GRSN)*, Michael Korn (Editor), Wiley, New York, 73–83 (http://www.geophys.uni-stuttgart.de/~widmer/wws.pdf).

Zürn, W., J. Exß, H. Steffen, C. Kroner, T. Jahr, and M. Westerhaus (2007). On reduction of long-period horizontal seismic noise using local barometric pressure, *Geophys. J. Int.* **171,** 780–796.

Black Forest Observatory
Universities of Karlsruhe and Stuttgart
Heubach 206
D-77709 Wolfach, Germany

Manuscript received 11 September 2008